Biomedicine & Pharmacotherapy 168 (2023) 115630

Contents lists available at ScienceDirect

Biomedicine & Pharmacotherapy

journal homepage: www.elsevier.com/locate/biopha

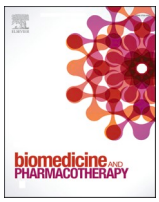

Circulating tumor DNA-based copy-number profiles enable monitoring treatment effects during therapy in high-grade serous carcinoma

Mai T.N. Nguyen [a], Anna Rajavuori [b], Kaisa Huhtinen [a,c], Sakari Hietanen [b], Johanna Hynninen [b], Jaana Oikkonen [a,*], Sampsa Hautaniemi [a,*]

[a] Research Program in Systems Oncology, Faculty of Medicine, University of Helsinki, Helsinki 00291, Finland
[b] Department of Obstetrics and Gynecology, Turku University Hospital, Kiinamyllynkatu 4, Turku 20521, Finland
[c] Institute of Biomedicine, University of Turku, Kiinamyllynkatu 10, Turku 20014, Finland

ARTICLE INFO

Keywords:
CtDNA
Copy-number alterations
Targeted sequencing
Treatment monitoring
High-grade serous carcinoma

ABSTRACT

Circulating tumor DNA (ctDNA) analysis has emerged as a promising tool for detecting and profiling longitudinal genomics changes in cancer. While copy-number alterations (CNAs) play a major role in cancers, treatment effect monitoring using copy-number profiles has received limited attention as compared to mutations. A major reason for this is the insensitivity of CNA analysis for the real-life tumor-fraction ctDNA samples. We performed copy-number analysis on 152 plasma samples obtained from 29 patients with high-grade serous ovarian cancer (HGSC) using a sequencing panel targeting over 500 genes. Twenty-one patients had temporally matched tissue and plasma sample pairs, which enabled assessing concordance with tissues sequenced with the same panel or whole-genome sequencing and to evaluate sensitivity. Our approach could detect concordant CNA profiles in most plasma samples with as low as 5% tumor content and highly amplified regions in samples with ~1% of tumor content. Longitudinal profiles showed changes in the CNA profiles in seven out of 11 patients with high tumor-content plasma samples at relapse. These changes included focal acquired or lost copy-numbers, even though most of the genome remained stable. Two patients displayed major copy-number profile changes during therapy. Our analysis revealed ctDNA-detectable subclonal selection resulting from both surgical operations and chemotherapy. Overall, longitudinal ctDNA data showed acquired and diminished CNAs at relapse when compared to pre-treatment samples. These results highlight the importance of genomic profiling during treatment as well as underline the usability of ctDNA.

1. Introduction

Copy-number alterations (CNAs) are commonly detected genomic aberrations in various types of cancer [1–4]. They can affect the activation or silencing of gene expression or pathway activities [5,6] and play a role in tumor initiation [3,7–9]. Several studies have detected CNAs to identify genomic changes driving to treatment resistance [10–12] and to gain insights into tumor evolution [9,11,13–15]. While the role of CNAs in cancer is indisputable, obtaining tissue biopsies for CNA analysis is not always feasible. Circulating tumor DNA (ctDNA) provides a minimally invasive biopsy technique for treatment monitoring and guidance [16–22].

High-grade serous carcinoma (HGSC) is the most common and deadliest subtype of epithelial ovarian cancer [23]. HGSC is considered as a copy-number-driven cancer with almost 100% prevalence of pathogenic mutations in *TP53* [24,25]. While the majority of HGSC patients respond to the primary treatment, cancer relapses in 95% of cases, eventually leading to chemotherapy resistant disease [26]. Previous ctDNA studies in HGSC have focused on longitudinal tracking of mutation profiles, with many methods for constructing subclonal populations based on mutations [27–29] and especially on *TP53* mutations [25,30,31], whereas CNAs have received less attention [25,30,31].

Detecting CNAs from cell-free DNA (cfDNA) poses challenges because of their low tumor fraction (TF). High TF requirements, such as the previously employed threshold of 25% [32] or 15% in our earlier study [16], led to the discarding a significant number of samples that

List of abbreviations: HGSC, High-Grade Serous Carcinoma; cfDNA, cell-free DNA; ctDNA, circulating tumor DNA; CAN, Copy Number Alteration; TF, Tumor Fraction; VAF, Variant Allele Frequency; PDS, Primary Debulking Surgery; NACT, Neoadjuvant Chemotherapy; ROI, Region of Interest; PoN, Panel of Normals.

* Corresponding authors.
E-mail addresses: jaana.oikkonen@helsinki.fi (J. Oikkonen), sampsa.hautaniemi@helsinki.fi (S. Hautaniemi).

https://doi.org/10.1016/j.biopha.2023.115630
Received 25 July 2023; Received in revised form 23 September 2023; Accepted 3 October 2023
Available online 6 October 2023

still can provide information. To address this issue, we conducted a study to detect CNAs in 152 plasma samples collected from 29 HGSC patients collected before and after treatments, including a substantial number of low TF cfDNA samples. Our study aimed to assess the feasibility of utilizing low-TF samples and investigate changes in CNAs during different treatment phases.

2. Materials and methods

2.1. Cohort and samples

Patients were selected from DECIDER cohort (NCT04846933) treated at Turku University Hospital (Turku, Finland). Patients were treated with either with primary debulking surgery (PDS) followed by platinum-taxane chemotherapy ($n = 14$), or neoadjuvant chemotherapy (NACT), where interval debulking surgery was performed after NACT, and followed by adjuvant chemotherapy ($n = 15$). Three patients in the NACT group did not undergo debulking surgery. All patients participating in the study provided informed consent and the study was approved by the Ethics Committee of the Hospital District of Southwest Finland (ETMK 145/1801/2015).

Samples included i) cfDNA from plasma, ii) genomic DNA from fresh frozen tumor tissue or ascites, and iii) genomic DNA from the blood of the same patient serving as a germline control. Sample preparation and DNA extraction protocols were performed as previously reported [16].

2.2. Deep sequencing of plasma samples and target regions

The samples were sequenced on an Illumina HiSeq platform using BGI Oseq™ ctDNA panel (Oseq panel) to target cancer-related genes. Plasma samples were sequenced with 1000x coverage, and genomic DNA from the tumor tissue and germline controls were sequenced with 200x coverage.

There were multiple batches of data, owing to the upgraded panels in the BGI. A panel of approximately 500 protein-coding cancer-related genes [16] (Supplementary Table S1) was used to successfully sequence 29 tissue samples, 100 plasma samples, and 15 germline control samples. Later, a larger panel of over 700 protein-coding cancer-related genes (Supplementary Table S2) was applied to 17 tissue, 52 plasma, and 16 germline control samples (Supplementary Table S3).

2.3. Tools and algorithms

2.3.1. Sequencing data processing

The quality control and alignment followed same procedures than previously [16] described and were based on GATK [33] best practice workflows in preprocessing sequencing data. After filtering for quality, 152 out of 166 originally sent plasma samples from 29 patients remained for analysis.

2.3.2. Identifying regions of interest (ROIs)

To identify regions of interest (ROIs) from the Oseq panel, we calculated coverage at every base of germline control samples ($n = 30$) and considered regions with a mean of coverage at least 100. Then, we excluded black-listed regions using ENCODE blacklist [34] and regions shorter than 200 bp. To curate the defined ROIs, they were checked with Integrated Genome Browser (IGB) [35] alignment visualization (Supplementary Fig. S1A) and the R package TarSeqQC [36] (Supplementary Fig. S1B). The final curated ROIs were then used for the CNA calling pipeline (Supplement Methods).

2.3.3. Estimation of ctDNA content in plasma samples

We used the truncal *TP53* variant allele frequency (*TP53* VAF) to estimate the ctDNA fraction for plasma samples. *TP53* VAF values were obtained by jointly calling all samples from a patient with GATK [33], version 3.7, with targeted option of gene region of *TP53*.

To gain further insight into the ctDNA fraction, we used Picard [37] to calculate the median fragment size and number of short (≤150 bp) and long (>150 bp) DNA fragments. Subsequently, we determined the short-long ratio by dividing the number of short fragments by the number of long fragments.

2.3.4. CNA pipeline

CNAs were called from the targeted sequencing data by using PureCN [38]. PureCN calculates coverage for each sample in the ROIs, corrects for GC content and mappability, and normalizes the coverages against Panel of Normals (PoN). Separate PoNs were used for plasma and tissue samples due to differences in background noise (Supplementary Methods). The workflow of the CNA calling pipeline for a single sample is shown in Supplementary Fig. S2. The segmentation profiles were visualized interactively on a web browser with GenomeSpy 40and as static figures using the R package copynumber [39].

From the CNA profiles, we calculated the CNA burden represented by focal and broad CNA signal scores (Supplement Methods) by using formula described by Franch-Expósito et al. [40].

2.4. Statistical analyses

Statistical analyses were performed using the R software (version 4.3.0). A threshold of 0.05 *p*-value was applied to define the significant statistical comparisons.

2.4.1. Comparison between samples

To compare the detected CNAs in tissue and plasma samples, we calculated concordances between samples with *TP53* VAF > 10% in tissue and > 1% in plasma, which resulted in 24 pairs of plasma and tissue samples from the same timepoints (Supplementary Table S4). Comparisons were performed using the Kendall correlation (R package 'stats') using the $\log_2 R$ ratio (logR) values of CNA segments between the matched tissue and plasma samples.

2.4.2. Associations between ctDNA and clinical factors

We applied linear regression and the Wilcoxon rank sum test from R package 'rstatix' to explore associations between ctDNA features and clinical factors.

2.4.3. Gene-level CNA status with GISTIC2 analysis

We run GISTIC2 analysis [41] for 29 pretreatment tissue samples to determine the prevalence of gene-level status. Gene-level scores resulting from GISTIC2 were used to infer the gene-level CNA status with thresholds of ± 0.5. The parameters for running GISTIC2 are specified in the Supplementary Methods.

2.5. Validation of ctDNA-Detected CNA Events Using Whole-Genome Sequencing (WGS) Samples

The comparative studies that show that WGS is reliable data source for CNAs and correlates well with more traditional approaches, such as FISH and IHC, have been conducted earlier [42,43]. Thus, to validate the CNA events identified in ctDNA, we leveraged copy-number profiles derived from 40 WGS samples obtained from 13 patients (Supplementary Table S5). These WGS data were previously generated as part of our recent study [14] and served as a reliable source for validating the observed CNA events.

3. Results

3.1. ctDNA detection and tumor fraction evaluation

We sequenced 152 plasma samples from 29 HGSC patients during their treatment (Fig. 1A) belonging to the DECIDER cohort (Table 1), expanding the previously published set of 12 patients [16]. Additionally,

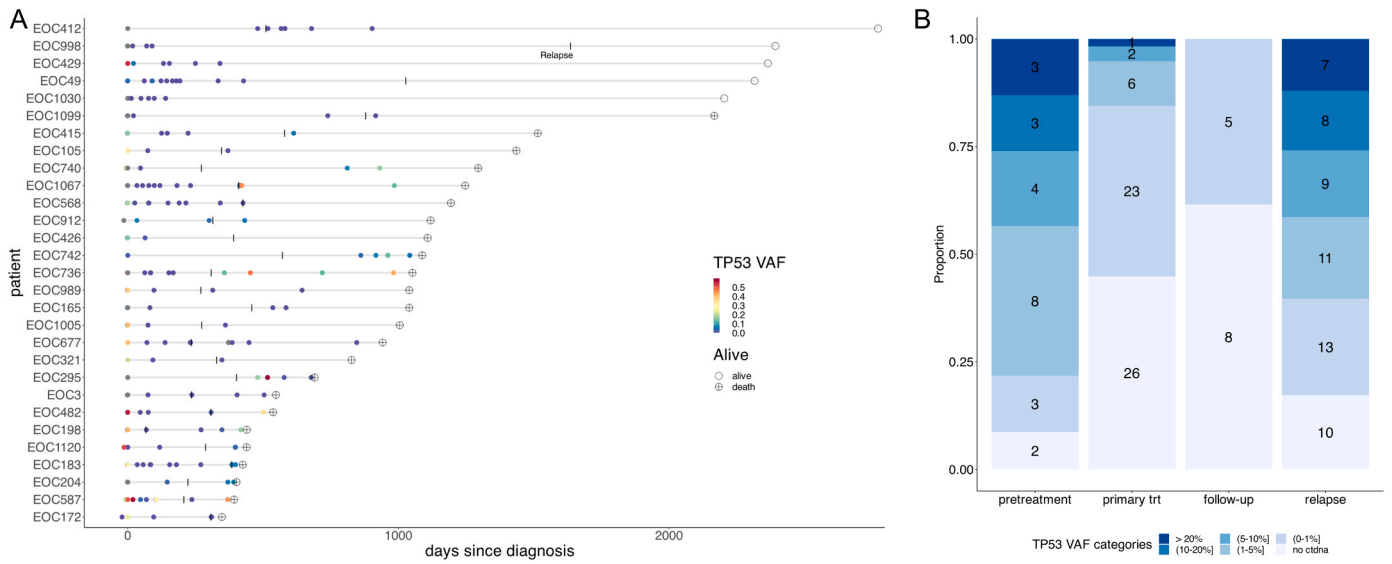

Fig. 1. Sampling and ctDNA detection along treatment phases. A) Timing of the sequenced samples for each patient is shown here with estimated TF (*TP53* VAF). Timing of first relapse is marked with vertical line. B) Proportion of samples with varying *TP53* VAF are shown for different treatment phases. trt = treatment.

Table 1
Summary of clinical factors in the cohort of 152 plasma samples from 29 patients. Plasma samples were collected at initial surgery (laparoscopy or PDS, called pretreatment here), during primary treatment, at follow-up, and at relapse.

Number of patients	29
Median age	68 (57 – 81)
Stage	
IIB	1
IIIC	19
IVA	5
IVB	4
Treatment strategy	
PDS	14
NACT	15
Average samples collected per patient	7 (3 – 24)
Plasma samples per treatment phase	
Pretreatment	23
Primary treatment	58
Follow-up	13
Relapse	58

46 tumor tissues and ascites samples were used for comparison and *TP53* mutation detection.

Most plasma samples had detectable ctDNA levels, as measured by *TP53* VAF [25,30,31] (70%, 106 samples). However, the ctDNA fraction (tumor fraction, TF) was generally low, most commonly less than 1% (90 samples), and only 22 samples (from 12 patients) had TP53 VAF > 10% (Fig. 1B). As expected, TF was the highest in the pretreatment (median *TP53* VAF 0.04) and relapse samples (median *TP53* VAF 0.029) (Fig. 2A), of which ~85% had detectable ctDNA (Fig. 1B).

We further examined the TF estimates, especially the use of DNA fragment sizes for plasma samples. Although cfDNA typically exhibits a median read length of 167 bp [44], ctDNA fragment sizes are generally shorter, ranging from 134 to 144 bp [44]. Thus, DNA fragment size proposes an independent measure for ctDNA proportion that is not influenced by *TP53* mutation status or its copy-number values. Consistent with *TP53* VAF, we observed longer median fragment sizes in follow-up and during primary treatment, indicative of lower tumor fractions (Fig. 2B). The correlation between *TP53* VAF and the short-long ratio (SLR) of ctDNA fragments in pretreatment samples was 0.84 ($p < .001$) (Supplementary Fig. S3A) while the correlations with SLR of relapse samples were not statistically significant (Supplementary Fig. S3B). Moreover, in a few samples during primary chemotherapy with low *TP53* VAF, we detected unexpectedly short median fragment sizes (Fig. 2B), possibly indicating an effect of chemotherapy on fragment length. Thus, *TP53* remained the primary TF estimate for further analyses, whereas DNA fragment size provided a complementary inference, specifically limited to pretreatment samples.

Furthermore, we explored the relationships between *TP53* VAF values in pretreatment and relapse ctDNA and various clinical factors, such as age at diagnosis, CA125 levels, cancer stage, and progression-free interval (PFI), categorized as either shorter or longer than six months. However, our analysis revealed that most clinical factors were not significantly associated with *TP53* VAF values (Supplementary Fig. S3 C,D,E,F). In conclusion, the studied clinical factors did not explain the detected variability between patients in ctDNA proportions in the plasma, even after pretreatment.

3.2. Detection of copy-number events depends on the ctDNA fraction of the plasma samples

To evaluate the sensitivity of CNA detection, we tested whether copy-number values ($\log_2 R$) correlated between matched plasma and tissue samples. As expected, correlations were highest in the high-TF samples (Fig. 2C, Supplementary Table S4). Most plasma samples with > 1% *TP53* VAF showed concordant CNAs with matched tissue samples (interactive visualization: https://csbi.ltdk.helsinki.fi/pub/home/nguyenma/GenomeSpy/publication/mnguyen_et_al_2023/?spec=spec.json#bookmark:Segmentation-from-tissue-and-plasma-samples). Most CNA profiles of plasma samples that had no detectable *TP53* VAF were flat and showed no CNAs (Supplementary Fig. S4), suggesting that the false positive signal rate was low. Overall, more CNAs were detected in higher TF samples, as shown in Fig. 2C,D.

CNA detection is most sensitive to highly amplified regions, which can also be detected also in low TF samples. As an extreme example, highest amplifications at *KRAS* and *CCNE1* in patient EOC740 were detected in plasma samples with *TP53* VAF as low as 0.4% (Supplementary Fig. S5, interactive visualization: https://csbi.ltdk.helsinki.fi/pub/home/nguyenma/GenomeSpy/publication/mnguyen_et_al_2023/?spec=spec.json#bookmark:High-signal-of-amplification-detected-with-purity-of-0.004-in-a-plasma-sample). Copy-number losses were more commonly missed in the lower TF samples.

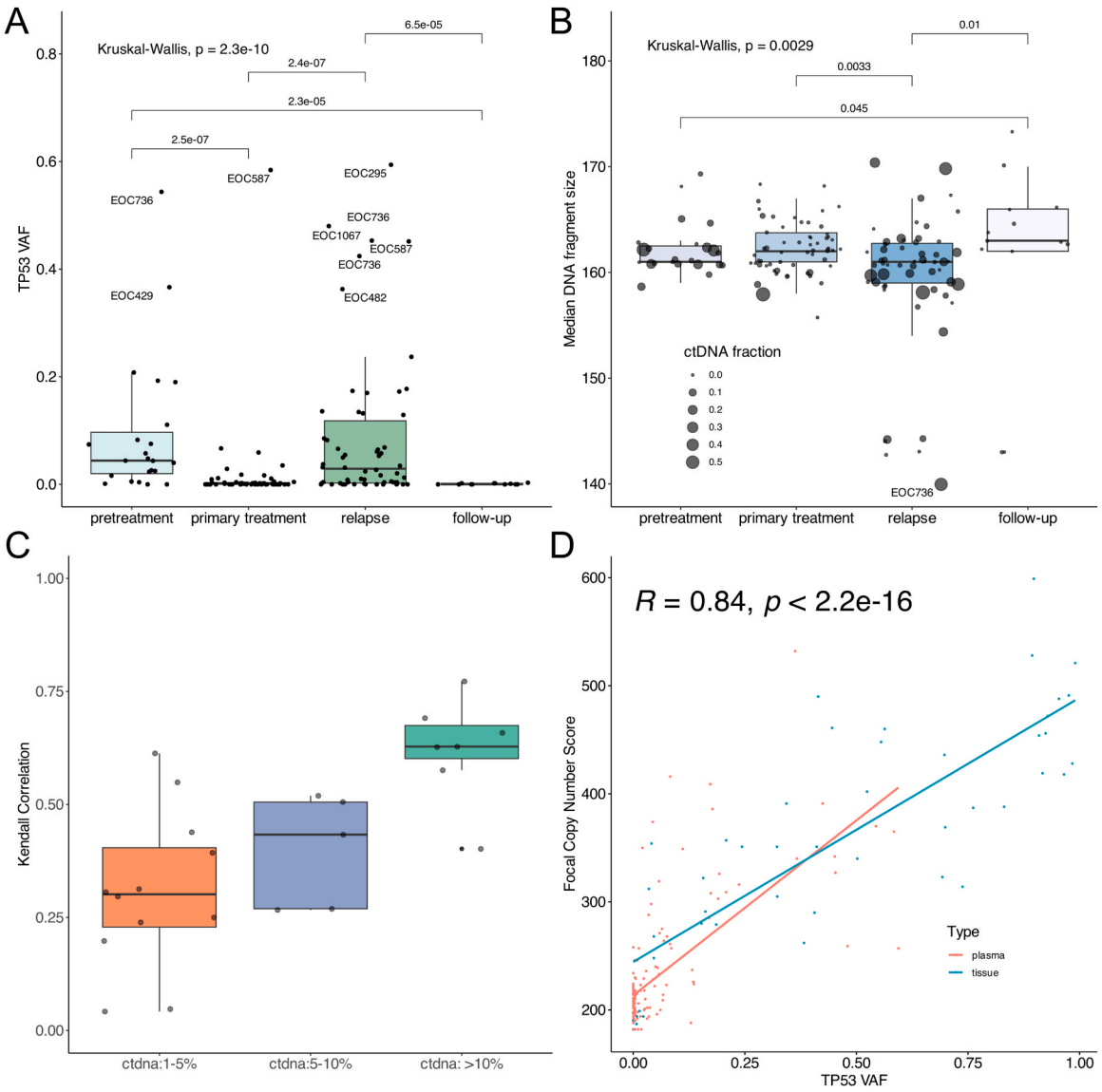

Fig. 2. Tumor fraction affects CNA detection. A) *TP53* VAF based TF estimates between different treatment phases. Only few samples have ctDNA detected at follow-up or during primary treatment. B) DNA fragment sizes vary accordingly between different treatment phases. However, median DNA fragment size-based estimates have poor concordance to *TP53* VAF based estimates after treatments. Especially at relapse, unexpectedly short median fragment sizes are detected in samples with varying *TP53* VAF values. (C) CNA profile correlation between matched ctDNA and tissue is affected by TF. (D) There is significant association between Focal CNA signal score, and *TP53* VAF of both tissue and plasma samples. Comparisons between 2 groups made with Wilcoxon.

3.3. Longitudinal copy number profiles showed genomic changes along the course of treatment

Because high copy-count amplifications can be detected most sensitively, we focused on studying the gene-level effects of *MECOM* (chr3q21), *MYC* (chr8q26), *KRAS* (chr12p21), and *CCNE1* (chr19q12), which are known oncogenes [3,23] and commonly amplified in patients with HGSC (Fig. 3A). Of note, *MECOM* region at chromosome 3 is sometimes referred as the *PIK3CA* region. Here, it is referred as the *MECOM* region since *MECOM* is the most frequently amplified gene in the region [14].

Examining the amplification statuses between the pretreatment tissue and plasma samples, we observed a predominantly concordant pattern (Fig. 3B). Most patients showed consistency in amplification status across both tissue and plasma samples. However, there have been a few discordant cases. For EOC1030, amplification was detected only in the ctDNA samples for *KRAS*, and for EOC587, amplification of *CCNE1* was also specific to the ctDNA samples and was not observed in the Oseq panel tissue samples. Interestingly, in the case of EOC204, two amplifications were detected on both sides of *KRAS*, but closer examination suggests that these might be spurious detections in the lower TF pretreatment plasma sample.

Moving beyond pretreatment analysis, we explored the changes in amplification profiles between pretreatment and relapse samples. Both acquired and lost CNAs were detected in these genes, indicating dynamic changes during treatment (Fig. 3B). Despite the overall concordance in profiles between the pretreatment and relapse samples, some patients exhibited notable differences. For example, EOC736 showed loss of *MECOM* and *MYC* amplifications and acquired *CCNE1* amplification. EOC587 showed loss of *MYC* and acquired *MECOM* amplifications. Heterogeneity in *MYC* and *CCNE1* amplification status longitudinally and between tissue biopsies has been detected in a recent study [45].

As an example, patient EOC587 showed focal changes during treatment. This patient had stage IV disease (Fig. 4A) and underwent diagnostic laparoscopy with removal of the ovaries, followed by neoadjuvant

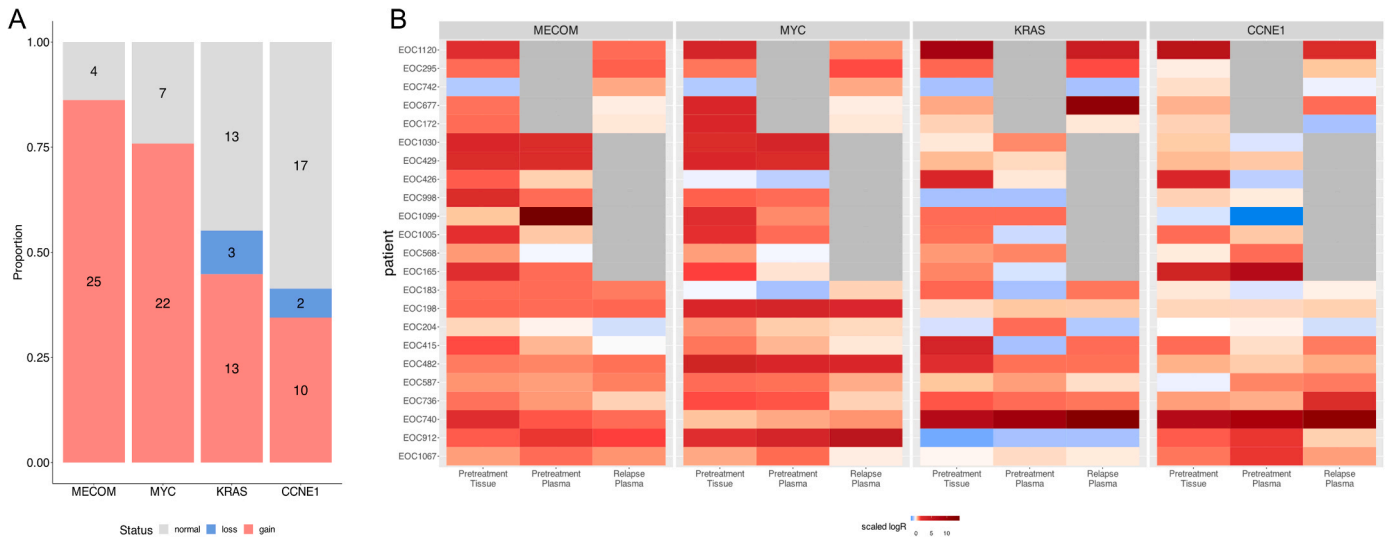

Fig. 3. : Heterogeneity and treatment effects at amplification statuses at *MECOM*, *MYC*, *KRAS*, and *CCNE1*. (A) The prevalence of copy-number events detected based on tissue biopsies at diagnosis in all 29 patients. (B) Comparison of amplifications between pretreatment and relapse as well as tissue and plasma. Plasma samples with TF in the range of 0.05–0.6 are shown here (7 samples with TF smaller than 0.1), resulting in 15 patients. LogR values were rescaled for third quantile for positive logR and absolute of first quantile for negative logR in each sample to allow comparison between samples of varying TF.

chemotherapy (NACT). However, progression occurred during adjuvant chemotherapy. The CNA profile remained the same for the most part, focal changes became apparent after laparoscopy and continued following chemotherapy (Fig. 4B). Her CNA profile in ctDNA samples changed during laparoscopy and again at relapse. An amplification at *PALB2* at chromosome 16 was acquired during laparoscopy and was recurrently detected at IDS from liver metastatic sample (Fig. 4B). In relapse plasma, this amplification was no longer detected and other acquired CNA events were detected instead. For example, acquired losses were detected on chromosome 14 (including *XRCC3* and *HSP90AA1*) and the entire p arm of chromosome 7.

We conducted a comprehensive analysis of CNA profiles in samples with *TP53* VAF exceeding 3% which showed focal CNAs, to assess heterogeneity and treatment effects ($n = 18$, Supplementary Figs. S6-S23). Among these, 11 patients (Supplementary Figs. S6-S16) had available tissue or plasma samples before treatment and after chemotherapy, enabling us to evaluate changes occurring during treatment. CNA profiles changed in the majority of patients; longitudinal changes in CNA profiles were detected in seven patients (Supplementary Figs. S6-S12), indicating treatment-induced alterations. In contrast, only two patients showed no detectable changes in their copy number profiles (Supplementary Figs. S13-S14). In two patients, the differences in the CNA profiles were not clearly discernible (Supplementary Figs. S15-S16). Notably, most high TF relapse plasma samples were collected close to death (less than 2 months before death), but these included both changing and stable CNA profiles.

It is important to highlight that even in patients with a plasma sample having a TF of only 3%, we were able to detect focal amplifications, as demonstrated by patient EOC1120 (Supplementary Fig. S11). This finding underscores the remarkable sensitivity of our approach for detecting genomic alterations, even at low TFs.

Notably, two patients, EOC482 (Supplementary Fig. S8) and EOC736 (Supplementary Fig. S10), displayed significant changes in their CNA profiles, which affecting multiple chromosomes. These patients initially achieved a complete response after receiving neoadjuvant chemotherapy (NACT) but experienced relapse within six months after primary treatment. Interestingly, in the case of EOC482, the altered CNA profile was detected at the second relapse, despite receiving no targeted treatments other than weekly paclitaxel and doxorubicin during the first and second relapses, respectively. Similarly, in the case of EOC736, the CNA profile changed between the diagnosis and the fourth relapse, following ctDNA-guided trastuzumab treatment during earlier relapses [16]. In particular, the *ERBB2* (*HER2*) amplification detected in the pre-treatment sample vanished after receiving targeted therapy and was not detected in the subsequent samples.

These findings provide compelling evidence for the dynamic nature of CNA profiles during treatment and highlight the potential of ctDNA analysis for tracking treatment response and detecting genomic changes associated with relapse. This emphasizes the importance of monitoring CNAs as a complementary tool to understand cancer cell evolution and treatment efficacy.

3.4. Detected CNAs match to tumor tissues with independent sequencing

To further validate the CNA findings, we used independent WGS of tumor tissue samples. This protocol ensured that the detected CNAs were not technical errors from the used sequencing nor ctDNA-related fluctuations but represented tumor CNAs.

In the commonly amplified regions (Fig. 3), 9 patients out of 12 were concordant with WGS data (75%; TF>5%; Supplementary Table S6): at least half of the WGS tissue samples in the same or closest timepoint had concordant CNA status. Particularly, ctDNA analysis missed at least one amplification in two patients (EOC415 and EOC165) and the third discordant patient (EOC1067) had an amplification at relapse, not detected at pretreatment tissue samples. Notably, patient EOC415, with a ctDNA TF of 4.8% at pretreatment, exhibited an amplification in *CDKN1B*, which was concordant with all three WGS pretreatment samples (Supplementary Table S7). Thus, all ctDNA-detected CNAs matched tissues from the same treatment phase.

Pretreatment WGS tissue data showed heterogeneity between anatomical sites in five occasions of which two were estimated normal and two amplified in pretreatment ctDNA. These results underscore both the validity of ctDNA findings and the advantage of ctDNA biopsies in capturing tissue heterogeneity [29,46].

Patient EOC740, with *KRAS* and *CCNE1* amplifications, and patient EOC1120 with *CCNE1* amplification, were detected at extremely low TF ctDNA sample (0.4% and 0.5% TF, respectively). These findings were consistent with the results from WGS tissue samples (Supplementary Table S7), highlighting the high sensitivity of our ctDNA-based CNA detection.

The *PALB2* amplification detected only during primary treatment at EOC587 (Fig. 4B) was similarly only detected in WGS tissues at interval

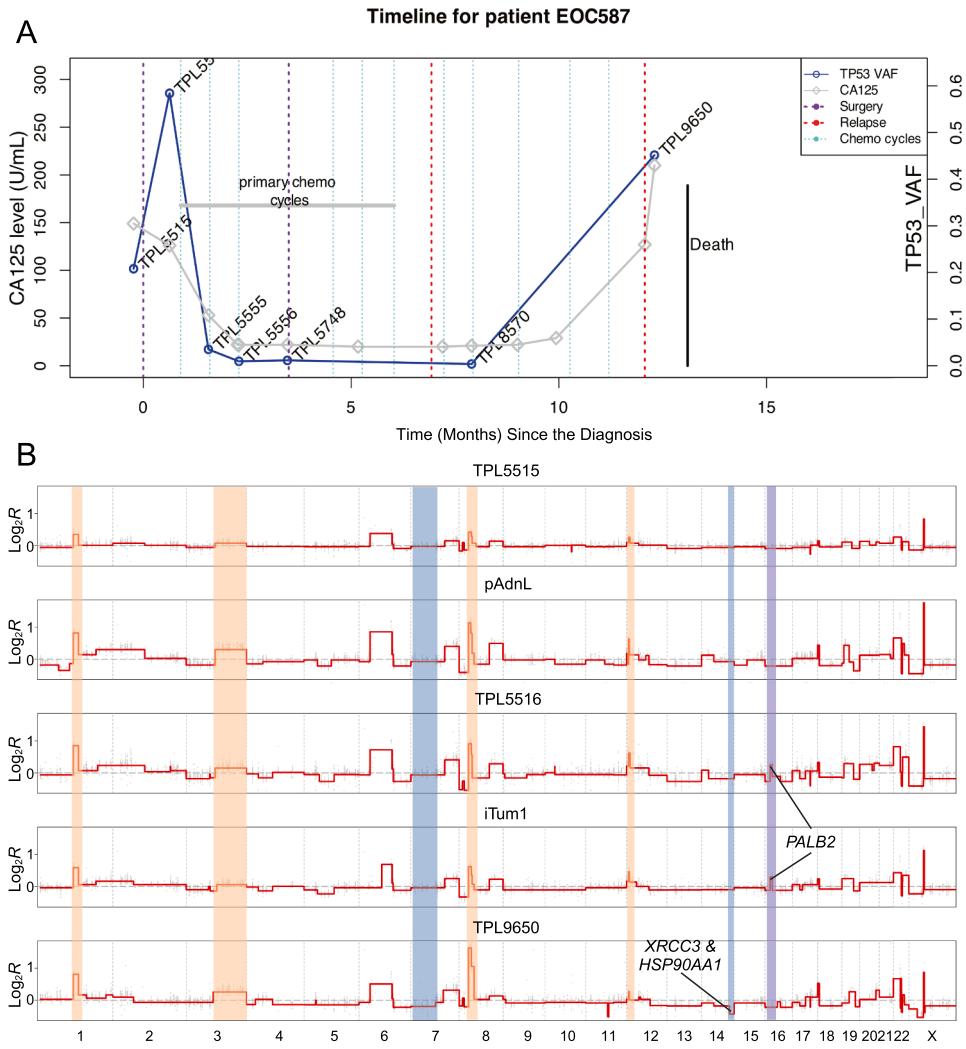

Fig. 4. : Tracking changes from longitudinal CNA profiles in a NACT treated HGSC patient along treatments. (A) Clinical timeline of patient EOC587 with CA125 and estimated plasma TF. (B) Longitudinal CNA profiles in tissue and plasma biopsies. Positive values denote amplified regions and negative values losses. Plasma samples during NACT and first relapse provided mostly flat signals, whereas pretreatment (*TP53* VAF = 20%), pre-chemotherapy (*TP53* VAF = 40%) and second relapse (*TP53* VAF = 45%) plasma samples showed well-defined CNA profiles. Orange highlighted regions denote recurrent amplifications, blue acquired losses at relapse and lilac subclonal amplification that was detected only during primary treatment. Tissue samples included pretreatment left adnexa (pAdnL) and interval liver metastasis (iTum1).

debulking surgery but not at primary adnexal or peritoneal tissue sample (Supplementary Table S7). Additionally, the deletions found only at relapse ctDNA, mainly *XRCC3* and chromosome 7p, were not detected at pretreatment or interval WGS tissues, strengthening their role as relapse-emerging CNAs.

4. Discussion

We assessed the utility of ctDNA for longitudinal CNA profiling in patients with HGSC. Our findings revealed that although the overall CNA profiles remained relatively stable, seven of the 11 patients exhibited focal genomic changes, primarily consisting of acquired and lost amplifications, during and after primary therapy. Importantly, even in a plasma sample with *TP53* VAF as low as 3%, we were able to detect CNA events. Moreover, two patients displayed extensive changes in their CNA profiles, affecting multiple chromosomes, between the pretreatment and relapse samples. This observation contrasts with a previous result that observed no changes in CNAs [47] with lower-resolution sequencing data.

Low ctDNA fractions may limit the usefulness of ctDNA, particularly for CNA calling. Here, we were able to detect high copy-count amplifications in a plasma sample with a TF of less than 1% (Supplementary Fig. S5). Generally, copy-number profiles are recognizable in samples with more than 5% ctDNA. Earlier studies have used the threshold of at least 20% tumor fraction for the analysis of ctDNA-based CNA [32,48], the higher sensitivity here allowed us to define signals for ctDNA-based CNA profiles for majority of patients (18 out of 29, Supplementary Fig. S6-S22). Moreover, most CNA events detected from ctDNA using the 5% TF threshold aligned well with the gold standard WGS data from tumor tissues [42,49], which suggests that ctDNA can serve as a source for monitoring genomic changes in cancer patients, especially when invasive tissue biopsies are not available.

The ctDNA fragmentation profile may be suitable for TF estimation of cfDNA samples [44,50,51]. However, our observations show poor correlation after chemotherapy between cfDNA fragment sizes in sequencing data and *TP53* VAF. Additionally, samples with unexpectedly low DNA fragment sizes without detected *TP53* VAFs did not have detectable CNAs. These results suggest that chemotherapy can affect cfDNA release from other cell types and alter cfDNA fragment sizes in plasma. Future studies focusing on fragmentomics-based approaches should evaluate these findings further.

Although our study demonstrates the potential of longitudinal

plasma ctDNA sampling for CNA profiling, we acknowledge limitations. First, the copy number calling approach used in this study, based on targeted sequencing, may not fully capture the entire genome's copy number profile, potentially leading to underestimation of genomic variation between samples. Therefore, it would be valuable to explore genome-wide approaches such as shallow whole-genome sequencing for further validation. Additionally, the small sample size of our study emphasizes the need for future validation using a larger cohort to confirm our findings.

We demonstrated that ctDNA can capture CNA information across different tumor sites and detect changes caused by surgeries and chemotherapies. ctDNA may reflect surgical removal of site-specific subclones, such as in the case of EOC587, chemotherapy-caused evolution between diagnosis and relapse, such as selection of resistant subclones due to treatment, such as loss of *ERBB2* amplification in the case of EOC736, or novel genomic events. These findings are in line with recent tissue-based studies by us [14] and others [45,46] showing subclonal heterogeneity at pretreatment and between pretreatment and relapse. Only two patients had major changes in the CNA profile, and similar major subclonal changes due to chemotherapy were rare in these studies, but heterogenic disease at relapse was commonly discovered [43,52].

Plasma samples offer a significant advantage in terms of availability, enabling the detection of genomic changes during treatment. They provide additional information during relapse, allowing for the estimation of heterogeneity [29,53] and a more detailed assessment of potential drug target abundance in the entire tumor. Despite the limitations posed by low ctDNA levels, our analysis demonstrated the potential of ctDNA sampling for monitoring changes over time during relapse. Overall, our study highlights the potential of ctDNA sampling in the development of tailored treatment plans that can improve patient outcomes. Personalized medicine for cancer patients relies on their ability to monitor genomic changes and changes in abundance. CtDNA, particularly during relapse, provides a unique opportunity to detect genomic targets and biomarkers in a timely manner. However, it is important to better understand patients with low TF and their tumors as well as to develop more sensitive methods to address this challenge.

Ethics approval and consent to participate

All patients participating in the study gave their informed consent, and the study was approved by the Ethics Committee of the Hospital District of Southwest Finland (ETMK 145/1801/2015).

Funding information

This project has been supported by Academy of Finland, Sigrid Jusélius Foundation, Sakari Alhopuron Säätiö, and the European Union's Horizon 2020 research and innovation programme under grant agreement No 667403 for HERCULES and No 965193 for DECIDER.

CRediT authorship contribution statement

M.T.N.N; Conceptualization, Methodology, Bioinformatics pipeline, Data analysis, Visualisation, Writing - Manuscript and supplements preparation. **J.H:** Methodology - Patient recruitment and Sample selection, Reviewing. **J.O;** Conceptualization, Writing- Reviewing and Editing, Supervision. **S.Ha;** Conceptualization, Reviewing, Supervision. **A.R, K.H, S.Hi**; Reviewing.

Declaration of Competing Interest

The authors declare that they have no known competing financial interests or personal relationships that could have appeared to influence the work reported in this paper.

Data Availability

Data will be made available on request.

Acknowledgements

We thank MSc Kari Lavikka for help in the GenomeSpy visualizations. Computing resources from CSC — IT Center for Science are gratefully acknowledged.

Consent for publication

Not applicable.

Appendix A. Supporting information

Supplementary data associated with this article can be found in the online version at doi:10.1016/j.biopha.2023.115630.

References

[1] Y.-C. Tang, A. Amon, Gene copy-number alterations: a cost-benefit analysis, Cell 152 (2013) 394–405.
[2] C.D. Steele, et al., Signatures of copy number alterations in human cancer, Nature 606 (2022) 984–991.
[3] T.I. Zack, et al., Pan-cancer patterns of somatic copy number alteration, Nat. Genet 45 (2013) 1134–1140.
[4] C.-Z. Zhang, D. Pellman, Cancer genomic rearrangements and copy number alterations from errors in cell division, Annu Rev. Cancer Biol. 6 (2022) 245–268.
[5] C.N. Henrichsen, et al., Segmental copy number variation shapes tissue transcriptomes, Nat. Genet 41 (2009) 424–429.
[6] X. Shao, et al., Copy number variation is highly correlated with differential gene expression: a pan-cancer study, BMC Med Genet 20 (2019) 175.
[7] B. Nguyen, et al., Genomic characterization of metastatic patterns from prospective clinical sequencing of 25,000 patients, Cell 185 (563–575) (2022), e11.
[8] D.M. Roy, et al., Integrated genomics for pinpointing survival loci within arm-level somatic copy number alterations, Cancer Cell 29 (2016) 737–750.
[9] S. Turajlic, et al., Deterministic evolutionary trajectories influence primary tumor growth: TRACERx Renal, Cell 173 (595–610) (2018), e11.
[10] Y. Han, et al., Genetic interaction-based biomarkers identification for drug resistance and sensitivity in cancer cells, Mol. Ther. Nucleic Acids 17 (2019) 688–700.
[11] F.C. Martins, et al., Clonal somatic copy number altered driver events inform drug sensitivity in high-grade serous ovarian cancer, Nat. Commun. 13 (2022) 6360.
[12] I. Dagogo-Jack, et al., Tracking the evolution of resistance to ALK tyrosine kinase inhibitors through longitudinal analysis of circulating tumor DNA, JCO Precis Oncol. (2018) 1–14, https://doi.org/10.1200/PO.17.00160.
[13] R. Gao, et al., Punctuated copy number evolution and clonal stasis in triple-negative breast cancer, Nat. Genet 48 (2016) 1119–1130.
[14] A. Lahtinen, et al., Evolutionary states and trajectories characterized by distinct pathways stratify patients with ovarian high grade serous carcinoma, Cancer Cell (2023), https://doi.org/10.1016/j.ccell.2023.04.017.
[15] J.R.M. Black, N. McGranahan, Genetic and non-genetic clonal diversity in cancer evolution, Nat. Rev. Cancer 21 (2021) 379–392.
[16] J. Oikkonen, et al., Prospective longitudinal ctDNA workflow reveals clinically actionable alterations in ovarian cancer, JCO Precis Oncol. (2019) 1–12, https://doi.org/10.1200/PO.18.00343.
[17] E. Heitzer, L. Auinger, M.R. Speicher, Cell-free DNA and apoptosis: how dead cells inform about the living, Trends Mol. Med 26 (2020) 519–528.
[18] J. Tabernero, et al., Analysis of circulating DNA and protein biomarkers to predict the clinical activity of regorafenib and assess prognosis in patients with metastatic colorectal cancer: a retrospective, exploratory analysis of the CORRECT trial, Lancet Oncol. 16 (2015) 937–948.
[19] J.-C. Stadler, et al., Current and future clinical applications of ctDNA in immuno-oncology, Cancer Res 82 (2022) 349–358.
[20] R. Said, N. Guibert, G.R. Oxnard, A.M. Tsimberidou, Circulating tumor DNA analysis in the era of precision oncology, Oncotarget 11 (2020) 188–211.
[21] E. Heitzer, I.S. Haque, C.E.S. Roberts, M.R. Speicher, Current and future perspectives of liquid biopsies in genomics-driven oncology, Nat. Rev. Genet 20 (2019) 71–88.
[22] D.W. Cescon, S.V. Bratman, S.M. Chan, L.L. Siu, Circulating tumor DNA and liquid biopsy in oncology, Nat. Cancer 1 (2020) 276–290.
[23] Integrated genomic analyses of ovarian carcinoma, Nature 474 (2011) 609–615.
[24] A.A. Ahmed, et al., Driver mutations in *TP53* are ubiquitous in high grade serous carcinoma of the ovary, J. Pathol. 221 (2010) 49–56.
[25] C.A. Parkinson, et al., Exploratory analysis of TP53 mutations in circulating tumour DNA as biomarkers of treatment response for patients with relapsed high-grade serous ovarian carcinoma: a retrospective study, PLoS Med 13 (2016), e1002198.
[26] S.J. Ritch, C.M. Telleria, The transcoelomic ecosystem and epithelial ovarian cancer dissemination, Front Endocrinol. (Lausanne) 13 (2022).

[27] M. Tarabichi, et al., A practical guide to cancer subclonal reconstruction from DNA sequencing, Nat. Methods 18 (2021) 144–155.
[28] G. Caravagna, et al., Subclonal reconstruction of tumors by using machine learning and population genetics, Nat. Genet 52 (2020) 898–907.
[29] L. De Mattos-Arruda, et al., Capturing intra-tumor genetic heterogeneity by de novo mutation profiling of circulating cell-free tumor DNA: a proof-of-principle, Ann. Oncol. 25 (2014) 1729–1735.
[30] S.R. Vitale, et al., TP53 mutations in serum circulating cell-free tumor DNA as longitudinal biomarker for high-grade serous ovarian cancer, Biomolecules 10 (2020) 415.
[31] Y.-M. Kim, et al., Prospective study of the efficacy and utility of TP53 mutations in circulating tumor DNA as a non-invasive biomarker of treatment response monitoring in patients with high-grade serous ovarian carcinoma, J. Gynecol. Oncol. 30 (2019).
[32] L. Paracchini, et al., Genome-wide copy-number alterations in circulating tumor DNA as a novel biomarker for patients with high-grade serous ovarian cancer, Clin. Cancer Res. 27 (2021) 2549–2559.
[33] G.A. Auwera, et al., From FastQ data to high-confidence variant calls: the genome analysis toolkit best practices pipeline, Curr. Protoc. Bioinforma. 43 (2013).
[34] H.M. Amemiya, A. Kundaje, A.P. Boyle, The ENCODE blacklist: identification of problematic regions of the genome, Sci. Rep. 9 (2019) 9354.
[35] N.H. Freese, D.C. Norris, A.E. Loraine, Integrated genome browser: visual analytics platform for genomics, Bioinformatics 32 (2016) 2089–2095.
[36] G.A. Merino, et al., TarSeqQC: Quality control on targeted sequencing experiments in R, Hum. Mutat. 38 (2017) 494–502.
[37] Picard. http://broadinstitute.github.io/picard.
[38] M. Riester, et al., PureCN: copy number calling and SNV classification using targeted short read sequencing, Source Code Biol. Med 11 (2016) 13.
[39] G. Nilsen, et al., Copynumber: efficient algorithms for single- and multi-track copy number segmentation, BMC Genom. 13 (2012) 591.
[40] S. Franch-Expósito, et al., CNApp, a tool for the quantification of copy number alterations and integrative analysis revealing clinical implications, Elife 9 (2020).
[41] C.H. Mermel, et al., GISTIC2.0 facilitates sensitive and confident localization of the targets of focal somatic copy-number alteration in human cancers, Genome Biol. 12 (2011) R41.
[42] P. Roepman, et al., Clinical validation of whole genome sequencing for cancer diagnostics, J. Mol. Diagn. 23 (2021) 816–833.
[43] D. Nava Rodrigues, et al., RB1 heterogeneity in advanced metastatic castration-resistant prostate cancer, Clin. Cancer Res. 25 (2019) 687–697.
[44] E. Chen, et al., Cell-free DNA concentration and fragment size as a biomarker for prostate cancer, Sci. Rep. 11 (2021) 5040.
[45] P. Cunnea, et al., Spatial and temporal intra-tumoral heterogeneity in advanced HGSOC: implications for surgical and clinical outcomes, Cell Rep. Med 101055 (2023), https://doi.org/10.1016/j.xcrm.2023.101055.
[46] S.L. Swift, S. Duffy, S.H. Lang, Impact of tumor heterogeneity and tissue sampling for genetic mutation testing: a systematic review and post hoc analysis, J. Clin. Epidemiol. 126 (2020) 45–55.
[47] G. Macintyre, et al., Copy number signatures and mutational processes in ovarian carcinoma, Nat. Genet 50 (2018) 1262–1270.
[48] G. Zhu, et al., Tissue-specific cell-free DNA degradation quantifies circulating tumor DNA burden, Nat. Commun. 12 (2021) 2229.
[49] A. Belkadi, et al., Whole-genome sequencing is more powerful than whole-exome sequencing for detecting exome variants, Proc. Natl. Acad. Sci. 112 (2015) 5473–5478.
[50] Y. Liu, et al., Increased detection of circulating tumor DNA by short fragment enrichment, Transl. Lung Cancer Res 10 (2021) 1501–1511.
[51] H.R. Underhill, et al., Fragment Length of Circulating Tumor DNA, PLoS Genet 12 (2016), e1006162.
[52] R. Fisher, L. Pusztai, C. Swanton, Cancer heterogeneity: implications for targeted therapeutics, Br. J. Cancer 108 (2013) 479–485.
[53] M. Jamal-Hanjani, et al., Detection of ubiquitous and heterogeneous mutations in cell-free DNA from patients with early-stage non-small-cell lung cancer, Ann. Oncol. 27 (2016) 862–867.